ABSTRACT

Joint Circuit and Waveform Optimization
for Next-Generation Radar

Casey S. Latham, M.S.E.C.E.

Mentor: Charles P. Baylis II, Ph.D.

Due to congested wireless radio spectrum, next-generation radar transmitters will need to be adaptive and reconfigurable in real time to share spectrum with wireless communication devices. Typical system optimization methods rely on separate optimization of the circuit and waveform, which can lead to an over-emphasis on one criteria. While the end result may be acceptable, the intermediate results may not be desirable for a real-time situation. In this thesis, a joint circuit and waveform optimization technique is demonstrated that is designed for use in a real-time reconfigurable radar transmitter. Measurement results are presented to show how joint circuit and waveform optimization allows for better intermediate results that allow real-time optimization to be utilized.

Joint Circuit and Waveform Optimization for Next-Generation Radar

by

Casey Sheldon Latham, B.S.E.C.E

A Thesis

Approved by the Department of Electrical and Computer Engineering

_____

Kwang Y. Lee, Ph.D., Chairperson

Submitted to the Graduate Faculty of
Baylor University in Partial Fulfillment of the
Requirements for the Degree
of

Master of Science in Electrical and Computer Engineering

Approved by the Thesis Committee

_____

Charles P. Baylis II, Ph.D., Chairperson

_____

Robert J. Marks II, Ph.D.

_____

Jonathan Rylander, Ph.D.

Accepted by the Graduate School

May 2018

_____

J. Larry Lyon, Ph.D., Dean

Page bearing signatures is kept on file in the Graduate School.

TABLE OF CONTENTS

LIST OF FIGURES

LIST OF TABLES

ACKNOWLEDGMENTS

I would like to acknowledge Dr. Charles Baylis and Dr. Robert Marks II for their help throughout the process. I was very fortunate to have the opportunity to start working in the research group as an undergraduate student. While it took me a while to get caught up and to make meaningful contributions to the research group, Dr. Baylis and Dr. Marks helped me along the way and always pushed me to do more than I thought I could do. If it were not for their help, I would not have even considered attending graduate school. I will be forever grateful for the opportunities they gave me.

The work presented in this thesis was funded by the National Science Foundation under grant number ECCS-1343316.

CHAPTER ONE

Introduction

In 2007, Apple Inc. introduced the world to the iPhone, a device that the company claimed would revolutionize the way we use our cell phones. When the device was released to the public, it was quickly adopted and became the "gold standard." Other companies, such as Samsung and LG, quickly developed smartphones to compete with the iPhone, leading to new excitement for the wireless industry. Over the next few years, smartphones were rapidly adopted, with the telecommunications infrastructure struggling to keep up with the increase in demand. This congested the network, leading to dropped calls and data connection failures. AT&T, for example, reported an 8,000% increase in mobile data volume from 2007 to 2010, leading to severe network capacity issues, as the smartphone uses "24 times the mobile data traffic of a conventional wireless phone" [1]. Additionally, these new devices were causing AT&T to use "up their spectrum at an accelerating rate" [1].

To combat the network issues, the United States Congress, along with President Barack Obama, directed the Federal Communications Commission (FCC) to act, which led to the creation of the National Broadband Plan of 2010 [2]. One of the goals of the plan was to increase the availability of mobile networks to the public. To achieve this goal, the FCC announced a plan to reallocate a total of 500 MHz of spectrum. The spectrum cited for reallocation exists in groups between 225 MHz and 3.7 GHz. While the allocation is good news for wireless customers, it is concerning for radar operators

because the S-band radar frequency allocation overlaps the spectrum cited for reallocation.

To avoid issues with radar interference, a next-generation radar system should work in the dynamic spectrum access paradigm. In dynamic spectrum access, a device changes its operating frequency based upon the spectral usage of surrounding devices. Several other parameters might also need to change dynamically, such as operating power and operating bandwidth. The operating power, for example, might change depending upon the devices operating in adjacent spectral bands. Since radars are high-power devices, it is important that the power in the adjacent spectral bands is low enough to avoid interference with neighboring devices. The next-generation radar will also need to take advantage of the amount of available bandwidth, which would be dependent upon the presence of devices in adjacent spectral bands. Maximizing the use of bandwidth will aid in various aspects of radar performance, such as target detection. The parameters mentioned above will change in real time, and the next-generation radar must be able to compensate.

In an effort to make the next-generation radar conform to the principles of dynamic spectrum access, an improvement in the optimizations is needed. Typical attempts at waveform and circuit optimization with radar applications are performed independently, where the waveform is optimized with little to no consideration for the circuit and vice versa. However, due to the link between the waveform and the circuit performance, optimizing one and then the other limits the capability of the algorithm. It is believed that optimizing the circuit and the waveform simultaneously will allow an improved performance overall. Additionally, jointly optimizing both the circuit and the

waveform should provide steady progress towards meeting all parameters and objectives, instead of fully optimizing one and then the other. Fully optimizing one parameter and then the other usually results in a solution that is not optimal for both waveform and circuit performance.

Sequential optimization is first examined. In sequential optimization, the circuit is first fully optimized. From the final circuit optimization point, the waveform is fully optimized. However, this might not lead to optimal performance for all objectives, as the circuit-then-waveform approach might favor one objective over the other. Joint optimization of the circuit and waveform is performed and compared with sequential optimization. Under the principles of joint optimization, the circuit and waveform are simultaneously optimized to find the best possible tradeoff between the circuit optimization and waveform optimization. This is expected to increase the overall performance, especially during the optimization process. Both sequential optimizations are compared, showing the advantages and disadvantages of each optimization.

CHAPTER TWO

Circuit Optimization

When discussing a cognitive radar system, there are two different aspects to think about: the circuit optimization and the waveform optimization. The circuit optimization is discussed in this chapter, with the waveform optimization being discussed in the following chapter. The first section discusses the background information related to the circuit optimization method used in this thesis, which is heavily based on the work of Fellows [3] [4] [5] [6] [7]. The second section overviews the state-of-the-art and related work.

Background

The power amplifier is often the largest consumer of power in a radar transmitter. As such, its efficiency determines the efficiency of the overall transmitter. Power-added efficiency (PAE) is defined as the ratio of the difference between the input and output RF power to the DC power input to the amplifier:

$$PAE = \frac{P_{out,RF} - P_{in,RF}}{P_{DC}} \times 100\%. \qquad (2-1)$$

PAE is a function of the load reflection coefficient, known as Γ_L, of the amplifier [8]. The load reflection coefficient is the reflection coefficient on the Smith Chart, Γ, taken on the load side of the amplifier. This is demonstrated in the block diagram of Figure 1. The load reflection coefficient, Γ_L, is the reflection coefficient looking through the output matching network. The Smith Chart is shown with measured PAE contours

for a FET device, such as the Microwave Technologies GaAs FET, in Figure 2. The location with the maximum PAE is shown on the right of the Smith Chart by the square. Each point on a given contour has the same PAE value, with the values decreasing the as the contours extend from the maximum. These contours can be plotted by performing an amplifier load-pull measurement or simulation. A measurement or simulation of PAE is performed at each green '+' in Figure 2, corresponding to different values of Γ_L throughout the Smith Chart. In this load-pull, a total of 292 points were measured to determine the PAE contours. The same process can be done for other quantities, such as gain, adjacent channel power ratio (ACPR), and output power.

While a full load-pull is very effective for determining the PAE maximum, it is far too time-consuming for real-time optimization in the field. A fast, measurement-based search is needed for such real-time reconfiguration applications. The gradient-based approach similar to that of Fellows [5] and Baylis [9] is used in this thesis. Figure 3 shows the basic operation of the gradient-based optimization in the complex Γ_L plane. Starting from the candidate point, the search takes a step in the direction of the nearest neighbors, one in the $Re(\Gamma_L)$ direction and one in the $Im(\Gamma_L)$ direction. At each point, the PAE is measured in order to determine the gradient.

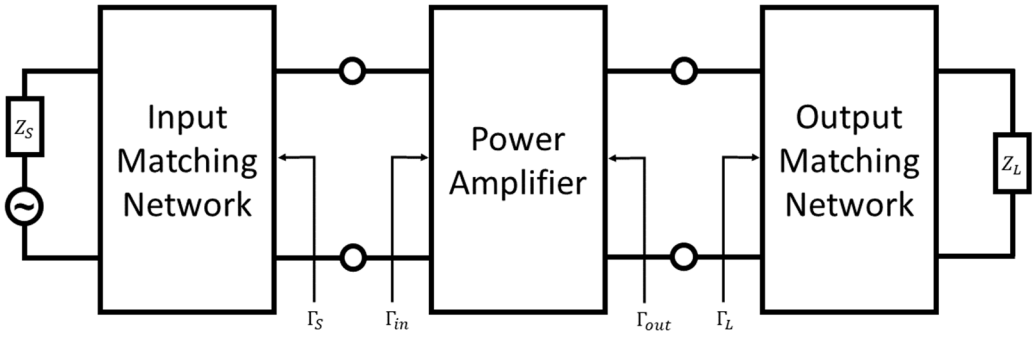

Figure 1. Block diagram of typical RF system

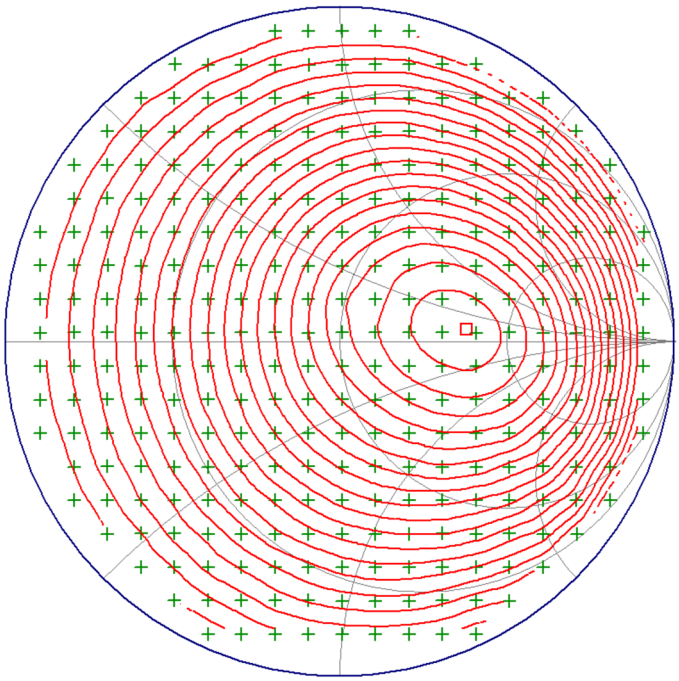

Figure 2. Example PAE contours. The maximum PAE contours for a FET device are shown in the Smith Chart, with each contour shown representing a specific PAE value.

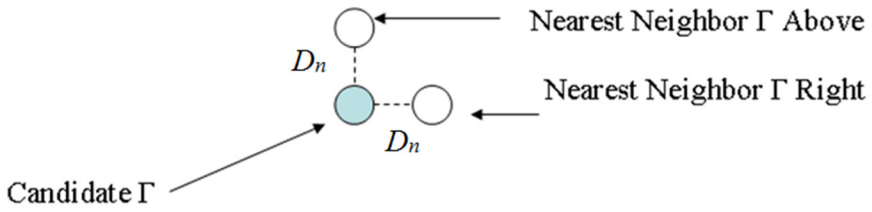

Figure 3. Gradient calculation. The nearest neighbor for each dimension is shown.

If PAE is represented by the variable p, the gradient for PAE, ∇p, is shown in terms of the unit coordinate vectors $\hat{\Gamma}_r$ and $\hat{\Gamma}_i$ using the equation

$$\nabla p = \hat{\Gamma}_r \frac{\partial p}{\partial \Gamma_r} + \hat{\Gamma}_i \frac{\partial p}{\partial \Gamma_i}. \qquad (2-2)$$

A unit vector in the direction of increasing PAE can be obtained by dividing ∇p by its magnitude

$$\hat{p} = \frac{\nabla p}{|\nabla p|} \qquad (2-3)$$

Because the search is one dimensional (as it only considers the PAE gradient), the search takes a step in the direction of the unit vector $\hat{p}$ with the maximum step size allowed, D_c. This is shown by the search vector $\bar{v}$ in the equation

$$\bar{v} = \hat{p} D_c. \qquad (2-4)$$

The search vector is added to the present candidate value of Γ_L to obtain the next candidate Γ_L. The initial value for D_c, which is the search step-size parameter, is set by the user. As long as the PAE at the next point is greater than at the current point, D_c stays at the maximum value. When the PAE at the next point is lower than at the current point, D_c at iteration i is divided by two and D_c becomes

$$D_{c,i} = \frac{D_{c,i-1}}{2} \qquad (2-5)$$

This process continues until the step size D_c is lower than the pre-specified minimum step size, D_{min}. When $D_c < D_{min}$, this indicates that the PAE has reached the maximum possible value. Therefore, the search stops and the PAE and final load reflection coordinates are reported.

State-of-the-Art in Circuit Optimization

This section consists of information regarding work that has already been done in the field of circuit optimization. Specifically, this applies to the idea of reconfigurable matching networks. H. Chen, et al. uses multi-mode power amplifiers that are able to reconfigure automatically into a lower saturated output power level, which will help save

energy [10]. This is different than the work done in this thesis, as the work in this thesis focuses on optimizing the load impedance of the matching network. D. Qiao, et al. uses a power amplifier with a reconfigurable output tuner using microelectromechanical system (MEMS) switches and a semiconductor-based varactor. The output tuner is designed to match a variety of load under a wide variety of conditions, including varying center frequency, output power, and load impedance. In order to optimize the tuner, pre-determined behavioral models and a characterization table are used to determine initial operating parameters. Depending on the fine tuning needed, either a simple output comparison or a genetic algorithm is used [11].

Fu and Mortazawi also explore using a power amplifier with a varactor-based reconfigurable matching network. In order to find the optimal tuner characteristics, a load-pull is performed in simulation and then a lookup table is used [12]. This is, however, not applicable to a true dynamic environment, as it is unrealistic to redo a simulation whenever the operating parameters change. Perez-Cisneros, et al. discuss a design with two reconfigurable matching networks using an architecture that allows for any number of different amplifiers to be used. In order to reconfigure the system, a 2-D vector quantization search is used, with the Smith Chart as the search space [13]. A. Semnani, et al. developed a high-power impedance tuner based upon evanescent-mode cavity technology that is controlled using a closed-loop control system [14]. N. Kingsley, et al. presents an adaptive amplifier module technique that is capable of significant improvements for demanding radio frequency applications, including cognitive radar. To control the adaptive amplifier module, the algorithm relies on a lookup table that would adjust the amplifier parameters [15].

The work contained in this thesis builds upon work that was done previously by Baylis, who discusses the ability to use a peak-search algorithm to calculate the peak power using a method that is less computationally-intensive than other searches [9]. This would save a substantial amount of time when testing new devices, especially if each device requires optimization.

Martin demonstrates an extension of this work, using a peak-search algorithm to first find the maximum PAE for a power amplifier, and then taking a small-step steepest descent walk on the Smith Chart to find the maximum PAE under a constraint on the adjacent-channel power ratio acceptable region (ACPR) [16]. This approach illustrates the Pareto optimization of power efficiency and spectral requirements, which has become very important with today's modern communication systems [17]. This work is furthered by Fellows, who discusses a direct optimization of PAE and ACPR [5]. This work is different than the work done by Martin, as this algorithm discusses a method of optimizing both the PAE and ACPR at the same time using a triangulation, vector-based approach rather than optimizing one criterion at a time. This work can be applied to power amplifiers in radar transmitters, which focused on improving the time it took to find the optimal load impedance [6].

Fellows furthers this work by adding another dimension to the Smith Chart, creating the Smith Tube. In addition to changing the load reflection coefficient, Fellows also shows that it is possible to change the bandwidth of a chirp waveform to improve the range radar resolution. The Smith Tube is used to visualize two-step search to find the optimal tradeoff of the load impedance and waveform bandwidth [7]. Barkate furthers the work of the Smith Tube by simultaneously optimizing the load reflection coefficient

and input power to optimize the PAE and ACPR, using a vector-based search reliant upon estimations of the PAE and ACPR gradients [18].

CHAPTER THREE

Waveform Optimization

The previous chapter discussed the circuit optimization, which was the first critical part of optimization techniques for a reconfigurable radar transmitter circuit. The other critical part is the waveform, as the waveform determines the resolution with which one is able to detect the position and speed of the target. The waveform optimization will be discussed in this chapter.

Background

For the waveform optimization, three goals are considered: (1) desired range and Doppler ambiguity function performance, (2) power-added efficiency maximization, and (3) spectral compliance. One of the most important functions used in radar systems is that of Woodward's ambiguity function, which is the output of the radar's correlation operation of the waveform $x(t)$ at delay displacement τ and Doppler displacement u from the actual delay and Doppler of the desired target [19]:

$$\chi_x(\tau, u) = \int_{-\infty}^{\infty} x(t)x^*(t-\tau)e^{-j2\pi ut}dt \qquad (3-1).$$

To find the optimal tradeoff between the three goals mentioned earlier, an optimization technique called alternating projections is used, which was explored by Eustice [20] [21] [22]. An illustration of the alternating projections approach is shown in Figure 4. If the projection starts from the red triangle, it projects onto the closest point on

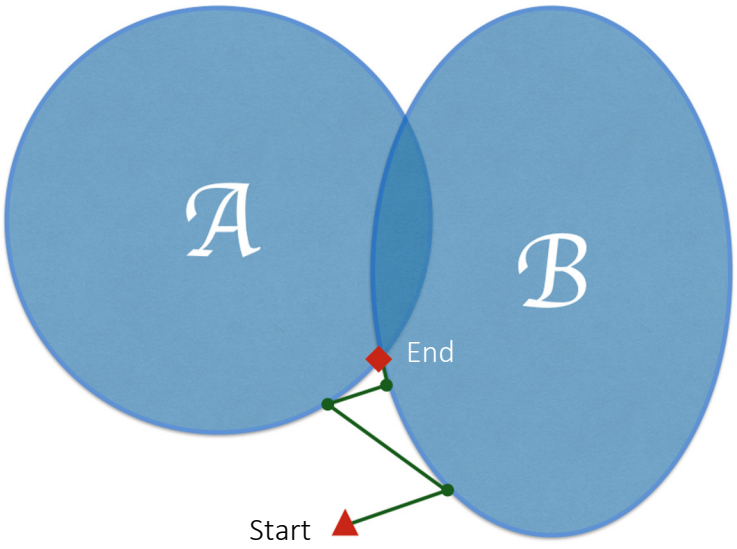

Figure 4. Alternating projections. An example of alternating projections between sets A and B.

the other set, set B in this case. From set B, the point is then projected onto the closest point of the other set, which is set A. The process repeats until it eventually converges to an intersection point of the sets. The end location is shown by the red diamond.

Alternating projections is a generalization of projection onto convex sets (POCS) approach. The only difference between alternating projections and POCS is that POCS necessitates that all of the sets are convex. By definition, a set, C, is convex iff for every vector $\vec{x}_1 \in C$ and $\vec{x}_2 \in C$, it follows that $\alpha\vec{x}_1 + (1-\alpha)\vec{x}_2 \in C$ for all $0 \leq \alpha \leq 1$ [23]. In other words, if any two points within *C* are connected by a straight line and this line is entirely enclosed within the set *C*, then the set is convex. This must be true for any two points within the set C. If the sets are not convex, then a unique solution is not guaranteed. For the alternating projections approach used in this work, the sets are not required to be convex. Empirically, most of the sets end up being approximately convex, which allows alternating projections to work fairly well.

When using alternating projections, three sets are used: (1) minimization function containing the 'ideal' ambiguity function, (2) peak-to-average power ratio, and (3) spectral constraints. First, the ambiguity function of the waveform is projected onto the minimization function $M(\tau, u)$ [20], which gives the result of

$$\frac{|\chi_x(\tau,u)|}{|\chi_x(0,0)|} \leq M(\tau,u). \qquad \begin{matrix} -B > u > B \\ -T < \tau < T \end{matrix} \tag{3-2}$$

This minimization function creates areas of minimization, where the ambiguity is to be minimal. The ambiguity function $\chi_x(\tau, u)$ projection onto the set of two-dimensional minimization functions **R**, which satisfy (3 – 2) [20], is given by

$$\Phi_x(\tau,u) = P_{\mathbf{R}}(\chi_x) = \begin{cases} \chi_x(\tau,u)\frac{M(\tau,u)}{|\chi_x(\tau,u)|}, & (\tau,u) \in \mathbf{B} \\ \chi_x(\tau,u), & (\tau,u) \notin \mathbf{B} \end{cases}, \tag{3-3}$$

where **B** is the set of range-Doppler combinations that do not satisfy (3 – 2).

An example minimization function for a range radar application is shown in Figure 5. The minimization function requires the ambiguity be confined to the red area along the Doppler axis, and requires minimal ambiguity in the blue areas. Low ambiguity equates to better resolution at the specific range-Doppler combination. The minimization function shown in Figure 5 is useful for providing high range resolution because the ambiguity is placed along the Doppler axis, which means that the range axis has more precision and can better detect the range of the target.

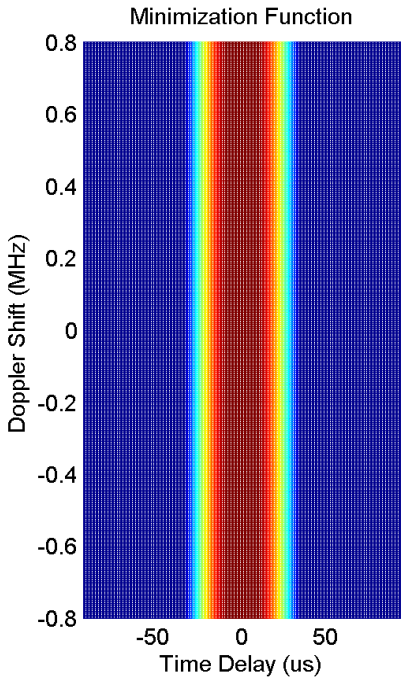

Figure 5. Example minimization function. This shows a minimization function for a range radar.

After the waveform is projected onto the minimization function, the optimization then projects the waveform onto the set containing all waveforms possessing peak-to-average-power ratio less than or equal to the requirement. Peak-to-average-power ratio (PAPR) is defined as

$$PAPR_{dB} = 10\log_{10}\left(\frac{P_{peak}}{P_{avg}}\right). \qquad (3-4)$$

The PAPR is limited because high efficiency waveforms typically have a lower PAPR. With a low PAPR, the amplifier can be set in high-efficiency mode for the peak, giving the remainder of the signal a high-efficiency input power. However, if the PAPR is high, the peak will operate with a high-efficiency input power, while the remainder of the

signal will be at a much lower-efficiency input power. Therefore, the overall efficiency will be lower [24].

After being projected onto the set of all waveforms meeting the PAPR requirement, the waveform is then projected onto the set of waveforms meeting spectral mask requirements. The spectral mask is a limit of the in-band radio frequency emissions of a transmitter, which would be a radar transmitter in this case. In the United States, the spectral mask is assigned to a specific user by the Federal Communications Commission (FCC) and the National Telecommunications and Information Administration (NTIA). An example of a spectral mask is shown in Figure 6. The thick red line in the figure is the limit for the radio spectrum. If the spectrum is above the red line, it is out of spectral compliance. If the spectrum is below or equal to the red line, it is in compliance. To quantify the spectral mask compliance, a metric S_m is used, which is defined as

$$S_m = \max(s - m), \qquad (3-5)$$

where s is the signal spectrum and m is the spectral mask. A positive S_m value would indicate a waveform that is not spectrally compliant for at least one frequency, while a negative S_m value would indicate a waveform that is spectrally compliant for all frequencies. Since any operation out of compliance would interfere with the radio's neighbors, spectral compliance is a requirement for the optimization. Under the POCS principle discussed earlier, if the frequency domain of the waveform is out of spectral compliance, any points that are out of compliance are pushed below the spectral mask.

Because the amplifier's output waveform (not the input waveform) must meet the ambiguity criteria, we desire to input a waveform that will produce the desired output after going through the nonlinear power amplifier. A model for the amplifier

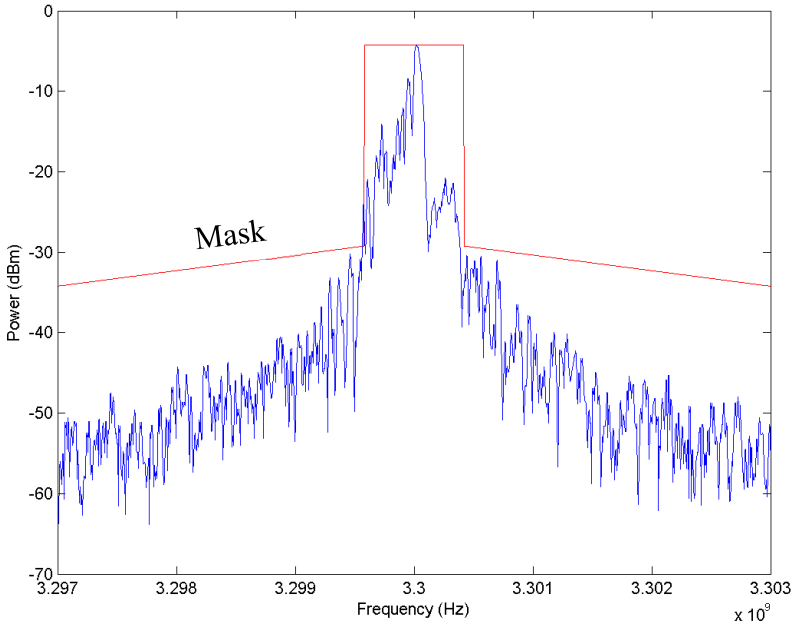

Figure 6. Example of a spectral mask. The spectral mask is shown in red.

nonlinearities is required for such input waveform synthesis. Currently, waveform optimization models the amplifier's output-voltage-versus-input-voltage characteristic as a hyperbolic tangent, as shown in [21]. Since the waveform optimization produces a waveform that is considered to be the ideal output, the hyperbolic tangent model is used to synthesize an input waveform that produces the desired output. The hyperbolic tangent model is shown in Figure 7. This is done because the amplifier exhibits nonlinearities, which cause the amplifier to distort the waveform in ways that are not taken into account in the normal waveform optimization. While the hyperbolic tangent model is simple, it works sufficiently well for 'on the fly' optimization in many cases due to the model's ease of extraction. This is discussed in detail by Eustice [22].

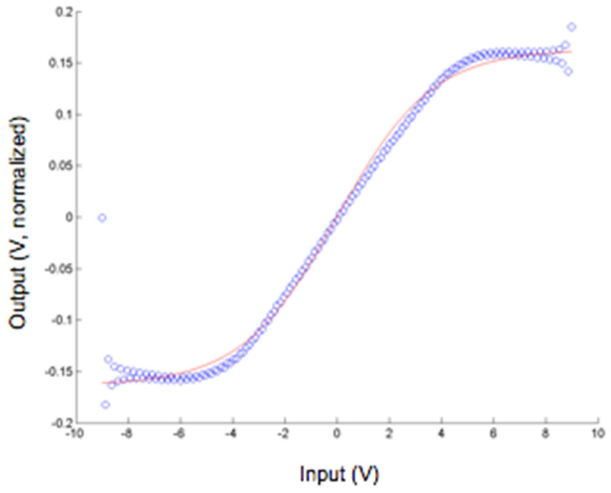

Figure 7. Example of the hyperbolic tangent model used for waveform optimization.

State-of-the-Art in Waveform Optimization

Other authors have used waveform optimization for radar-related research. Chen et al. discuss using each element of a multiple-input multiple-output (MIMO) radar to transmit an arbitrary waveform [25]. Modifying the waveform that each transmitter transmits allows the combined output waveform to be more complex than what any single transmitter is able to transmit. In addition, this would allow the waveform to optimize the signal-to-noise-interference ratio on each iteration. Synthesis with radar applications has been considered since the ambiguity function was introduced by Woodward in 1953 [19]. Early work in ambiguity function synthesis includes a technique by Wilcox, where a least squares estimation is used to create a waveform made up of basis function whose cross-ambiguity function approximates some goal cross-ambiguity function [26]. Sussman furthers this work by synthesizing ambiguity functions by minimizing the integrated square error between the desired function and an ambiguity function [27]. Wolf et al. works on an alternative approach for cross-ambiguity functions, instead using a pattern search and basis functions [28]. More modern

approaches by Gladkova and Chebanov further the work by Wilcox [29] [30]. Using alternating projections in waveform synthesis has also been demonstrated in previous literature. Kassab et al. also uses alternating projections for radar waveform synthesis, but instead focuses on the autocorrelation properties of the waveforms and does not consider the entire plane of the ambiguity function [31]. Yang et al. use an idea presented in a previous paper, where minimum mean-square error and mutual information are optimized to find the best MIMO radar waveform pattern. Alternating projections in now used to find the waveform solutions that can satisfy a structure constraint and optimize the design criteria [32]. Liu et al. examines using alternating projections to achieve high-velocity resolution and estimation accuracy for the pulse-train radar presented in this paper [33]. In more recent work, Blunt et al. uses projections and a similar amplifier-in-the-loop approach to radar waveform synthesis [34]. The projections used by Blunt et al. projects between sets focused around the peak sidelobe level and spectral content, instead of ambiguity function criteria. The method also focuses on continuous-phase-modulation to optimize both the peak and integrated sidelobe levels. However, the approach only benefits detection in nearby range resolution.

Most of the waveform optimization used in this thesis relates to the work done by Eustice in [20] [21] [22]. This work has been discussed in great detail in the previous section. The work of Eustice has also been extended [35], where Latham uses the waveform optimization discussed in the previous chapter and creates an algorithm that creates a dynamic spectral mask. The dynamic spectral mask is dependent upon the locations and operating frequencies of devices operating within the radar's band.

CHAPTER FOUR

Circuit and Waveform Optimization

State-of-the-Art in Circuit and Waveform Optimization

While substantial work has been done in both circuit and waveform optimization, not much work has been done to bring the two optimizations together. Chen et al. discusses using joint optimization of both the waveforms and receiving filters for a multiple-input multiple-output (MIMO) setup. The iterative algorithm optimizes both the waveform and the receiving filters to maximize the detection performance [25]. This work is not directly applicable to this thesis, as the receiving filters are being optimized, as opposed to the impedances. Nijsure et al. uses mutual information between subsequent radar returns to "extract desired information" from the radar's operating environment. Under this approach, the radar is constantly learning about its surroundings and modifies operating mode accordingly, thus creating a joint optimization between the radar's waveform and operating mode [36]. This work is also not directly applicable to the work presented in this thesis, as the amplifier's operating mode is changed, as opposed to the impedance.

Hardware-in-the-loop optimization is different than joint optimization. Hardware-in-the-loop is a method where the hardware's effects on the other aspects of the system are taken into consideration. For example, when considering amplifier-in-the-loop optimization, the amplifier's impact on the waveform is measured and used to improve the output waveform. Most work that uses an amplifier-in-the-loop approach has been developed by Professor Shannon Blunt and colleagues. Significant work has been done

in the exploration continuous phase modulation-based (CPM) waveform optimization, and hardware-in-the-loop integration. Jakabosky et al. demonstrates the ability to use continuous phase modulation-based waveforms for radar applications to create low sidelobes, as CPM-based waveforms have a peak-to-average-power ratio of 0 dB by design. This allows for high efficiency [37] [38]. This work was then applied to a hardware-in-the-loop optimization setup. Using a similar method of CPM-based optimization, Seguin et al. uses a hardware-in-the-loop optimization that includes the entire transmit chain [39]. The methods of model extraction are different than those used in this thesis. The authors use a model to characterize the amplifier before the amplifier is used. This limits the amplifier's ability to change impedances. Since the amplifier's nonlinearities change as the impedance changes, the model will need to be re-extracted at each impedance. This issue makes the model impractical for use in a joint optimization scenario, where load impedances are changing as the waveform changes. Joint optimization necessitates that the amplifier's model be re-extracted whenever the circuit optimization takes a step. Additionally, these methods are different than the work presented in this thesis, as the methods of radar waveform synthesis by these authors do not allow for the creation of an arbitrary waveform, instead confining the waveform to a fixed modulation scheme.

Blunt et al. have also explored using greedy search to optimize based on the peak sidelobe level, integrated sidelobe level, and spectral content to give low range sidelobes. Distortion due to the transmitter is also incorporated into the optimization using modeling and hardware, which allows for spectrum management [40] [34]. This method is also different than the method presented in this thesis, as it examines optimizing the peak and

sidelobe levels and spectral content and only benefits detection of targets in nearby range resolution. Because this method deals mostly with the sidelobe levels, it would not be feasible for methods which necessitate the use of arbitrary waveforms, especially waveforms that are very different from the range radar waveform. The work presented in this thesis focuses on optimizing the waveform for any arbitrary ambiguity function. This allows the waveform optimization to be flexible and considers more than the peak and sidelobe levels.

Experimental Setup

The optimizations were run on a test bench setup controlled by MATLAB, which controls a Maury Microwave load-pull tuner and a Keysight Technologies arbitrary waveform generator. Measurements were taken from a Keysight Technologies signal analyzer and power sensor. The test bench setup, with equipment labeled, is shown in Figure 8. The load tuner shown is different from the one used for this thesis, as the one shown is a Maury Microwave load-pull tuner. Two different amplifiers were used: a Microwave Technologies (MWT) High Gain GaAs FET and a Skyworks InGaP packaged amplifier. Two amplifiers were tested to ensure that the optimizations showed the same trends on different devices. The optimizations were also tested at various load reflection coefficients (Γ_L) around the Smith Chart to ensure that a variety of linearity regions were examined.

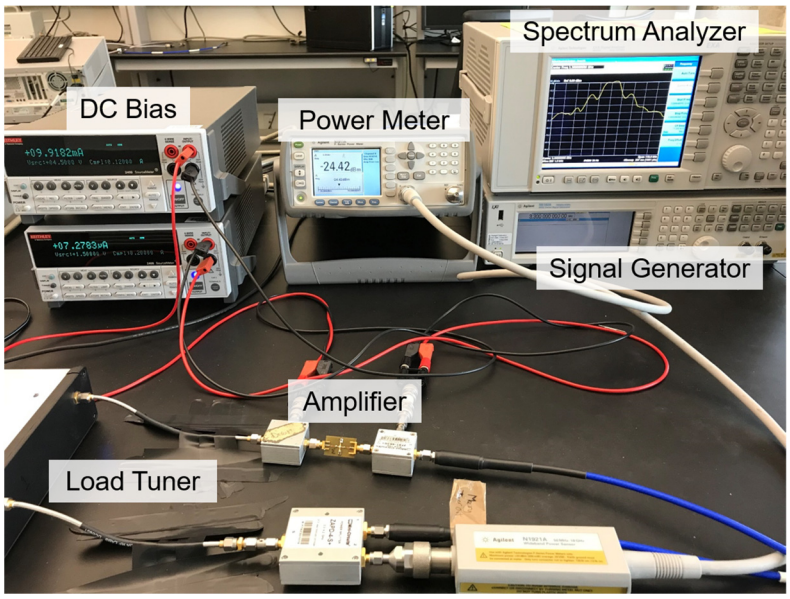

Figure 8. Test bench setup

Optimization Specifics

The initial waveform used in the optimization is defined as a complex exponential. It was previously determined that a relationship exists between the waveform's PAPR and the peak efficiency point on the Smith Chart. For this experiment, most of the waveforms used during the optimizations have a PAPR close to or exceeding 2 dB. Therefore, a waveform with a PAPR of less than 1 dB is used as the starting waveform. The baseband waveform is defined as

$$x(t) = \frac{e^{j\omega t}}{2} + e^{-j\omega t}, \qquad (4-1)$$

which has a PAPR of around 1 dB. The waveform $x(t)$ is modulated onto the carrier frequency. The PAPR of the starting waveform is well below the PAPR obtained for the final waveforms from the optimization. For example, the waveform produced when using the range radar minimization template shown in Figure 5 has a PAPR that is near the 7 dB limit.

Two different optimizations were explored: sequential and joint optimization. For purposes of this comparison, sequential optimization is a complete circuit optimization followed by a complete waveform optimization using the final load reflection coefficient Γ_L resulting from the circuit optimization. Starting from the initial Γ_L with the waveform defined in (4 – 1), a circuit optimization is completed to find the point on the Smith Chart that yields the highest PAE. The value of Γ_L is then fixed, and the waveform optimization is run for 40 iterations, with the first five waveform iterations being simulated on the computer. The simulated waveform iterations allow the waveform optimization to start heading in the right direction before being introduced into the measurement environment. Joint optimization is different than sequential optimization since it alternates between circuit and waveform optimization. Joint optimization starts with the same waveform that was defined in (4 – 1), followed by five waveform iterations that are simulated on the computer. Since these first five waveforms are simulated, they stay the same each time the optimization is run. Five waveform iterations are first performed, followed by one step in the circuit (Γ_L) optimization. The process repeats until a total of forty waveform iterations are completed. This means that a circuit step is taken after waveform iterations 10, 15, 20, 25, 30, 35, and 40. After the fortieth waveform iteration, the circuit search continues without any waveform optimization iterations until the circuit search converges. Once this happens, five more waveform optimization iterations are completed, allowing the waveform to be optimized for the final circuit location.

Sequential Optimization

When looking for the peak PAE operating point, the process of performing a circuit optimization is much quicker than a full load-pull measurement. While the two find the same maximum PAE point, the circuit optimization part of sequential optimization can obtain a result with significantly fewer measurements. The load-pull for the Microwave Technologies (MWT) amplifier is shown in Figure 9(a). The PAE maximum for the MWT amplifier is shown by the red square, which is located at 0.17/-23.99°. Another load-pull measurement was performed for the Skyworks amplifier, and is shown in Figure 9 (b). The PAE maximum for the Skyworks amplifier is also shown by the red square, which is located at 0.38/5.14°. Both load-pull measurements were performed with the same waveform, as defined by (4 – 1). This was done to maintain consistency between all optimizations.

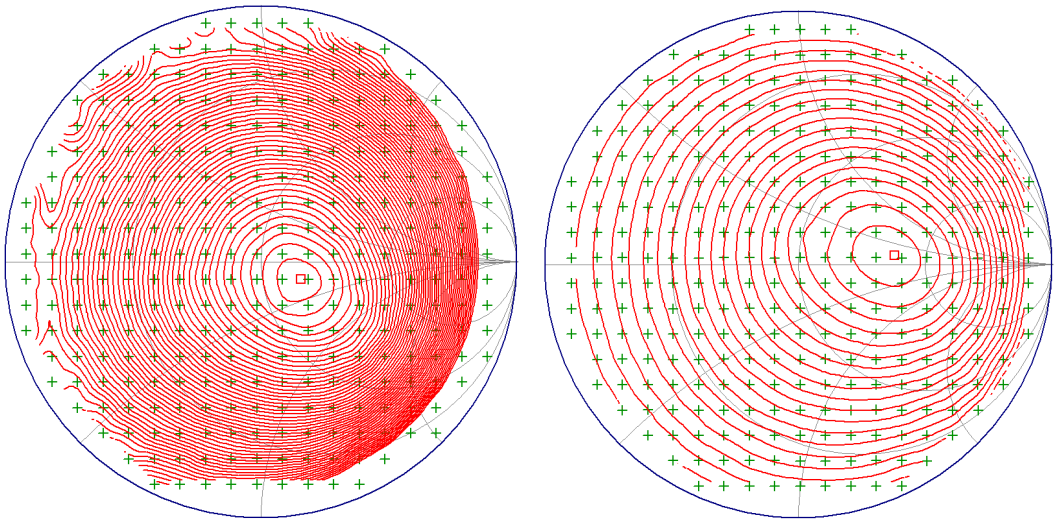

(a) (b)

Figure 9. PAE load-pull comparison. (a) Load-pull for the MWT amplifier, showing the maximum PAE point, indicated by the red square. (b) Load-pull for the Skyworks amplifier, showing the maximum PAE point, indicated by the red square.

The circuit search measurements from sequential optimization are compared to full load-pull measurements, with both the load-pull and circuit optimization using the same waveform as defined in (4 – 1). This is done because both the load-pull and circuit search from sequential optimization both find the PAE maximum; doing the circuit search is just a much faster way of doing so. The measurements are shown in Table 1, with the results sorted by the starting location and the type of amplifier. The ending Γ_L locations are shown, which indicates the PAE maximum for the given amplifier. These searches end at Γ_L values that are close to the maximum PAE points according to the load-pulls of Figure 9. This is demonstrated by the average distance between the full load-pull maximum Γ_L and ending Γ_L for the sequential optimization. For the MWT amplifier, the average distance was 0.016. For the Skyworks amplifier, the average distance was 0.0296. Looking at the Smith Chart, these distance values demonstrate that a circle with the radius equal to the average distance can be drawn around the PAE maximum determined by the load-pull. The average sequential optimization ending Γ_L would fall within this circle. This is further shown in Figure 10, which shows an example of the circuit optimization for the MWT amplifier with a starting reflection coefficient (Γ_L) of 0.8/-45°. Each step the circuit search takes is shown by a green square. As Figure 10 shows, the points all move in the same general direction, aside from one point, which steps just slightly outside of the path. This is most likely due to a drastic change in the linearity of the amplifier at that specific point on the Smith Chart. Despite the linearity change, the circuit search compensates and ends at a point that is close to the maximum PAE point shown in Figure 9(a).

Table 1. Sequential Optimization Runs for MWT and Skyworks Amplifiers

Starting Location	Optimization	Amp	PAE (%)	Sm (dBm)	WF LS Distance	Ending Location
0.8/0°	Sequential	MWT	-0.267	2.401	0.099685	0.17/-27.18°
0.8/45°	Sequential	MWT	0.028	0.953	0.099689	0.17/-39.84°
0.8/90°	Sequential	MWT	1.310	1.188	0.098980	0.16/-31.55°
0.8/180°	Sequential	MWT	-0.063	0.952	0.100368	0.22/-30.37°
0.8/-90°	Sequential	MWT	0.851	3.398	0.098867	0.16/-26.91°
0.8/-90°	Sequential	MWT	-0.842	0.741	0.098988	0.14/-28.19°
0.8/-45°	Sequential	MWT	-0.364	5.136	0.100764	0.21/-41.00°
0.8/90°	Sequential	SKY	2.562	-2.996	0.105097	0.39/3.80°
0.8/180°	Sequential	SKY	2.625	-5.319	0.105303	0.45/7.45°
0.8/-90°	Sequential	SKY	2.456	-0.816	0.104933	0.37/12.97°

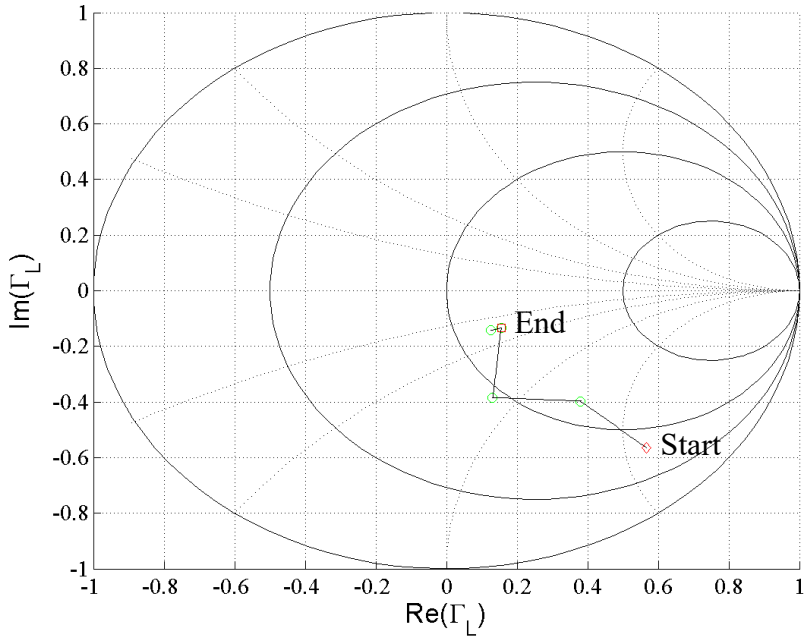

Figure 10. Circuit optimization for the MWT amplifier using sequential optimization. This shows the circuit optimization for the MWT amplifier starting from 0.8/-45°, finding the point of the maximum PAE.

Once the circuit optimization identified the maximum PAE Γ_L, a full waveform optimization was completed using this Γ_L value. These results are also recorded in Table 1. For most of the results, the PAE is negative, and for all cases, the PAE is very low. This is because the minimization function template used was working to optimize a range radar. After the circuit optimization is complete, the PAE that is achieved is relatively high, usually around 30% for the MWT amplifier. However, this is using the starting exponential, not the range radar waveform. Once the waveform starts to change to look more like the range radar, it immediately drops. This drop makes sense, as the starting waveform has a duty cycle of 100%. Intuitively, duty cycle is defined as:

$$D = \frac{t_{on}}{t_{period}} \times 100\%. \qquad (4-2)$$

Even though the starting exponential waveform has a duty cycle of 100%, the final waveform does not. Range radars use a time-domain pulse, leading to a waveform that has duty cycle of 10%-15%. Since the PAE is calculated over one whole period, the substantial amount of off time decreases PAE, because the DC bias power is still being used. The negative values shown above are due to P_{out} being lower than P_{in}. This is concerning because an amplifier should yield gain. However, P_{in} is read from the signal generator and is a single value of the average power. When the duty cycle is 100%, this would accurately match P_{in} over the whole signal. Because the duty cycle is around 10%-15%, P_{in} would be much lower for a significant part of the waveform. This would cause it to appear as if P_{in} is greater than P_{out}, which would cause the PAE to be negative. This is a problem for most of the data taken, but it is worse for the MWT

amplifier because it operates at a higher power level than the Skyworks amplifier. Such a problem could be corrected by pulsing the bias supply on and off with the RF waveform.

The S_m value that was recorded for the MWT amplifier experiments was also greater than 0, indicating that the final waveform was not spectrally compliant. This was due to limitations in the hyperbolic tangent predistortion model that was used. These limitations are primarily centered around the same duty cycle issue, as mentioned above with PAE. The hyperbolic tangent model is applied in the time domain, mapping the points from the time domain waveform to different points along the hyperbolic tangent model. However because the waveform is a pulse in the time domain (with a low duty cycle), the waveform doesn't map extremely well onto the hyperbolic tangent model, as this would lead to points being mapped to the extremes of the model, where it is less accurate. This can lead to some nonlinearities being excluded from consideration. Since these issues are mostly related to the low duty cycle of the waveform, these issues shouldn't be as prevalent for waveforms with higher duty cycles. Additionally, these issues could be fixed by a more adaptive predistortion model.

Lastly, the waveform (WF) least squares (LS) distances were all around 0.10 (unitless since this is a difference ratio between the output waveform and the minimization function template), which indicates that the output ambiguity function is very close to matching the minimization function in all cases. The least squares distance can be defined as

$$LS = \text{mean}(|M(\tau,u)| - |\chi(\tau,u)|)^2, \qquad (4-3)$$

where $M(\tau,u)$ is the minimization function template and $\chi(\tau,u)$ is the ambiguity function, and the quantities are averaged over all dimensions to achieve one result. A

least squares distance of 0.00 would indicate that the ambiguity function exactly matched the minimization function, and a least squares distance of 1.00 would indicate that the ambiguity function didn't match the minimization function at all. A value under approximately 0.11 is considered to be acceptable, as any waveforms with a least squares distance value of 0.11 has components reminiscent of a Doppler radar waveform, which is the opposite of a range radar. The comparison between the minimization function template and the ambiguity function for the starting Γ_L of 0.8/-45° (using the MWT amplifier) is shown in Figure 11. The origin of the ambiguity function is 0 dB, which is the maximum of the ambiguity function. The dark blue areas, which correspond to areas of low ambiguity, are at -50 dB. As shown in the figure, the ambiguity function places most of the ambiguity (shown in red) along the Doppler axis, which corresponds to a range radar. Because a PAPR limit of 7 dB was applied to the waveform optimization, it

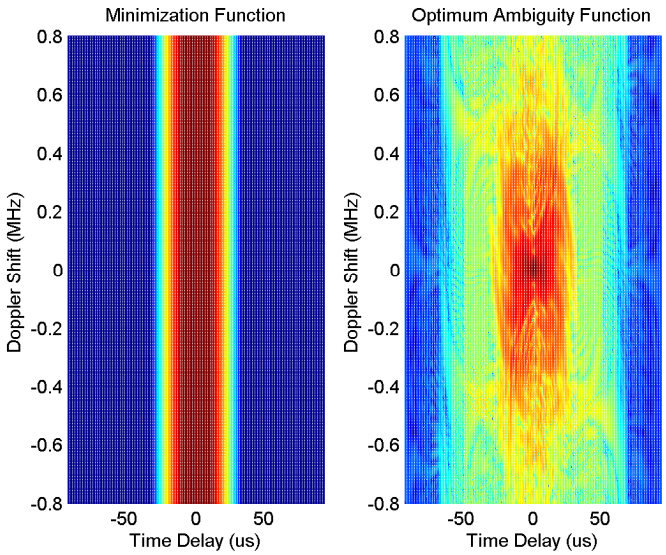

Figure 11. Sequential optimization for the MWT amplifier. This shows the waveform optimization for the MWT amplifier starting from 0.8/-45°.

is difficult to obtain an ambiguity function that matches the minimization function template exactly.

Joint Circuit and Waveform Optimization

While sequential optimization performs the circuit optimization first and then completely optimizes the waveform, joint optimization operates in a manner that allows for a tradeoff between the waveform and circuit. As discussed at the beginning of the chapter, the first five waveform optimizations are performed by a computer in simulation environment. This is done to save time and to allow the optimization to start working towards its ideal waveform from the start. After these initial five waveforms, five additional waveform iterations are completed using measurements, followed by a circuit step in the direction of the PAE maximum. The process of completing five waveform iterations and then taking a circuit step is continued for a total of 40 waveform iterations. This means that one circuit step is taken after waveform iterations 10, 15, 20, 25, 30, 35, and 40. After the fortieth waveform iteration, the circuit search continues until convergence. Upon convergence, five additional waveform optimization iterations are performed to ensure that the waveform is spectrally compliant at the final value of Γ_L. This also allows the waveform optimization to consider the nonlinearities that are present at the final Γ_L value.

The results from joint optimization are shown in Table 2. The main thing to notice about the data is the ending Γ_L value for each of the amplifiers. The ending Γ_L values are different than what was shown in the load-pulls shown in Figure 9. For the MWT amplifier, the average distance between the final Γ_L value and the PAE maximum

Table 2. Joint Optimization Runs for MWT and Skyworks Amplifiers

Starting Location	Optimization	Amp	PAE (%)	Sm (dBm)	WF LS Distance	Ending Location
0.8/0°	Joint	MWT	0.773	-0.380	0.100338	0.05/107.42°
0.8/45°	Joint	MWT	0.544	2.924	0.100444	0.04/73.69°
0.8/90°	Joint	MWT	1.118	1.777	0.098203	0.10/101.41°
0.8/180°	Joint	MWT	1.344	1.021	0.098439	0.07/119.82°
0.8/-90°	Joint	MWT	0.040	-0.122	0.103056	0.04/-159.9°
0.8/-45°	Joint	MWT	1.428	1.558	0.100809	0.04/71.87°
0.8/90°	Joint	SKY	2.727	2.322	0.103724	0.40/-23.37°
0.8/180°	Joint	SKY	2.863	0.203	0.105356	0.41/-18.26°
0.8/-90°	Joint	SKY	2.737	-3.293	0.105735	0.45/-12.32°

determined by the load-pull was 0.236. For the Skyworks amplifier, this distance was 0.163. While the ending reflection coefficients from sequential optimization all matched up well with the load-pulls, the data from joint optimization does not. Since the load-pull uses a different waveform than joint optimization, the maximum PAE Γ_L for the load-pull is not the same as the final Γ_L for joint optimization. This is because joint optimization is alternating between waveform and circuit optimizations. Therefore, the final Γ_L for joint optimization is the best tradeoff between the circuit and waveform. Because joint optimization is alternating between the circuit and waveform optimizations, the tradeoff allows the waveform to find the point on the Smith Chart that allows the algorithm to reach a point with a higher PAE, while still maintaining similar waveform least squares distance performance, when compared to sequential optimization.

Something else to note regarding the data shown in Table 2 is the fact that the PAE is low. Like sequential optimization, a range radar minimization template was used. Range radars normally have a lower efficiency than other radars (such as Doppler radars), so the low PAE from this algorithm does not indicate an issue with the optimization. The S_m is also greater than 0, which indicates that the waveform is not spectrally compliant at

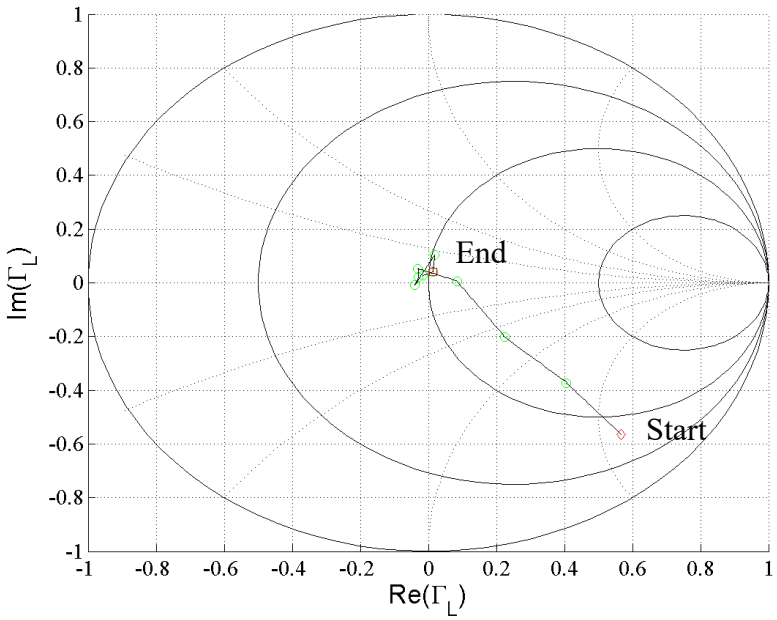

Figure 12. Circuit optimization for the MWT amplifier using joint optimization. This shows the circuit optimization for the MWT amplifier starting from 0.8/-45°, finding the point of the maximum PAE.

the output. Rather than being a limitation of the optimization, the lack of spectral compliance indicates a limitation with the hyperbolic tangent nonlinearity model. As discussed in an earlier section, because the range radar waveform has a low duty cycle, the hyperbolic tangent model can only compensate for some of the nonlinearities, making the model less effective.

Additional insight results from examining how the circuit search performed in joint optimization. An example of a circuit search is shown in Figure 12, where joint optimization was done using the MWT amplifier with a starting location of 0.8/-45°. As expected, the search path used to get to the maximum PAE point was largely straight. However, the algorithm loses some of the straightness as it gets closer to the PAE maximum. This is because as the circuit search gets closer to the PAE maximum, the circuit search step size gets smaller. Because the steps are smaller, joint optimization can

make more minute adjustments to both the circuit and the waveform, ensuring that the circuit and waveform match well.

Comparison of Joint and Sequential Optimizations

Table 3 shows a comparison between joint and sequential optimization. Shown in the table are the averages of all the trials, including data from additional trials not shown in the other tables within the previous sections. The main difference between joint and sequential optimization is shown by the ending reflection coefficient (Γ_L). There is a substantial difference between the ending Γ_L for sequential optimization and joint optimization. This is shown by the last column of Table 3, which indicates the average distance between the ending Γ_L value of the optimization and the PAE maximum determined by a load-pull. For both the circuit search of sequential optimization and the load-pull, the same exponential waveform, as defined by (4 – 1) was used. Sequential optimization performs the circuit search first, and then does the waveform optimization. Joint optimization, on the other hand, performs alternates between circuit and waveform optimization. Because joint optimization experiences a tradeoff between the circuit and waveform optimizations instead of trying to strictly maximize the PAE with a fixed waveform, the ending Γ_L values are different from the load-pull and the average distance is higher.

Table 3. Comparison of Joint and Sequential Optimizations

Optimization	Amp.	PAE (%)	S_m (dB)	WF LS Distance	Ending Location	End Γ_L Std. Dev.	Distance (Γ_L and load-pull)
Sequential	MWT	0.314	1.570	0.099	0.17/-29.38°	0.0352	0.016
Joint	MWT	2.205	2.437	0.100	0.07/126.57°	0.0571	0.236
Sequential	SKY	2.548	-3.044	0.105	0.40/7.96°	0.0522	0.0296
Joint	SKY	2.776	-0.256	0.105	0.42/-17.76°	0.0486	0.1630

Table 3 also shows the PAE values that the optimization generates. For both amplifiers, the PAE was higher for joint optimization, again due to the waveform and circuit tradeoff. The spectral mask compliance metric (S_m) also shows that joint optimization pushes the boundaries of the spectral mask more than sequential optimization. This is also due to the waveform and circuit tradeoff, as both the waveform and the circuit optimizations are pushing the boundaries of the spectral mask; the waveform optimization pushes the boundaries of the spectral mask due to the alternating projections (of which spectral compliance is a set). It should be noted that the neither of the averages of the optimizations for the MWT amplifiers resulted in a spectrally complaint output. As stated in the previous section, this is because the range radar waveform has a low duty cycle, causing the predistortion model to map less accurately to the hyperbolic tangent model. This limits the model's ability to compensate for nonlinearities.

While Table 3 allows for comparisons of the final values of important metrics, the true utility of joint optimization is shown through comparison of intermediate values during the optimization. Figure 13 compares least squares distance, which is the difference between the ambiguity function and the minimization function, for joint and sequential optimizations over time, using a metric called 'Equivalent Waveform Iterations'. Since five waveform iterations are taken for each circuit step in joint optimization, one circuit step is assumed to equal to five equivalent waveform iterations. This is based on estimated time required for the circuit and waveform parts of the search. Circuit steps are shown by lines covering the iterations over which the circuit step was performed, while waveform optimization is shown by squares for joint optimization and

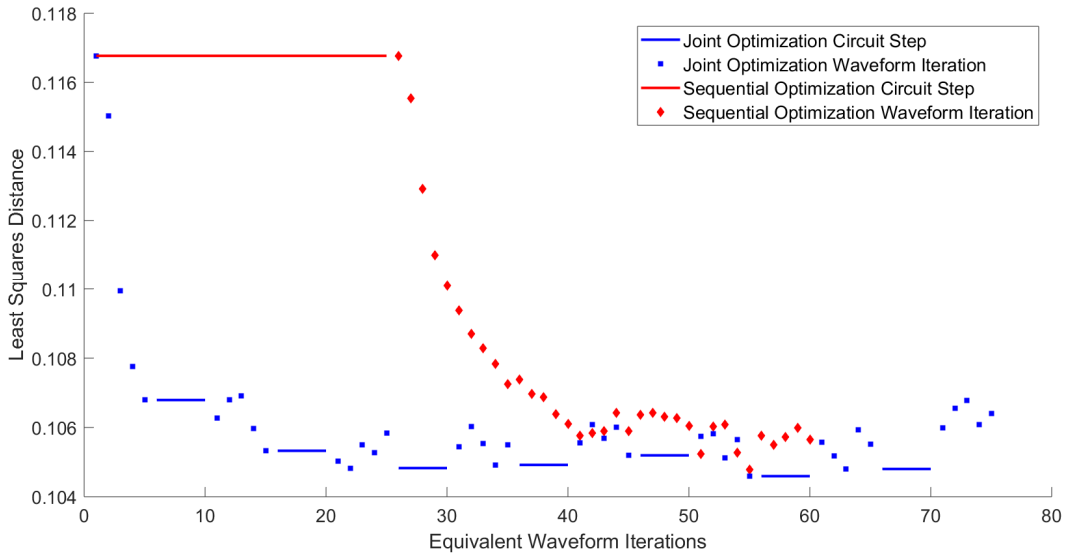

Figure 13. Least Squares Distance Comparison with Equivalent Waveform Iterations. This shows how the least squares distance performs throughout the optimizations for a typical joint and sequential optimization trial.

diamonds for sequential optimization. Since the least squares distance is a waveform metric, the least squares distance is only shown for the waveform optimizations. For the circuit steps for sequential optimization (shown by a red line), the least squares distance shown is the least squares distance of the starting waveform. For the circuit steps for joint optimization (shown by blue lines), the least squares distance shown in the plot is the least squares distance of the waveform that was used to start the circuit optimization, even though small fluctuations are expected in the least squares distance as the circuit search moves around the Smith Chart.

When looking at sequential optimization, the circuit optimization took 25 equivalent waveform iterations, which is equal to five circuit steps. These circuit steps were taken using the starting waveform, which has a least squares distance of approximately 0.1168. After the circuit search converged at iteration 25, the waveform optimization began from the final Γ_L. Five waveform iterations were then performed in a

simulation environment on the computer and are not shown in any of the optimization plots (for joint optimization, these simulated waveforms are done before the first five measurement-based waveform iterations and are not shown in the plots either). Thirty-five waveform iterations were then sent through the measurement setup. After 60 equivalent waveform iterations, the search completed.

Joint optimization is different. Because both the circuit and waveform are changing at the same time, joint optimization takes more circuit steps than sequential optimization. This leads joint optimization to take a slightly longer time to complete the algorithm run, which is limited to a total of 45 waveform iterations. Both joint and sequential optimization end with a similar least squares distance, with joint optimization being slightly higher because the final Γ_L is a tradeoff between the circuit and waveform. However, because joint optimization does waveform iterations first, the waveform immediately starts improving. Before sequential optimization even starts improving the waveform, the waveform for joint optimization far outperforms the sequential optimization waveform. In fact, by equivalent waveform iteration 26, joint optimization far exceeds the ambiguity function performance of sequential optimization.

Ambiguity function performance is demonstrated in Figure 14. This shows the waveform for each optimization at the intermediate equivalent waveform iteration 26. At this point, sequential optimization has completed the circuit optimization and the five simulated waveforms, with the ambiguity function of the first output waveform shown in the figure. Joint optimization has already completed several waveform iterations, with equivalent waveform iteration 22 shown, as it has the lowest distance from iterations 21 to 25 and is used for the circuit optimization. Sequential optimization has a least squares

distance of 0.1168, and joint optimization has a least squares distance of 0.1048. While the distance may seem small, it is substantial. When examining Figure 14, the joint optimization waveform shows much better agreement with a range radar. Sequential optimization shows some agreement with a range radar, but not much. Instead, the sequential optimization waveform is a good waveform to use for Doppler resolution, but would yield very poor range resolution. This would lead to low resolution detection of targets position.

The PAE comparison of joint and sequential optimization is shown in Figure 15. For sequential optimization, the circuit steps show that the circuit optimization (using the starting exponential waveform) improved the PAE until it arrived at the maximum PAE Γ_L. This maximum is close to the highest efficiency the Skyworks amplifier is able to achieve. Once the sequential optimization started to perform waveform optimization, the efficiency substantially decreased. This is because a range radar has a low duty cycle of about 10%. This substantially decreases the efficiency (a time domain impulse function has a very low PAE because the peak-to-average-power ratio is higher). Additionally, since waveform optimization doesn't try to improve the PAE, waveform optimization is limited by the PAPR. Therefore, the efficiency isn't being read from the test setup during the waveform optimization. Whenever the waveform optimization discovered a waveform with a lower least squares distance, it took a new PAE and S_m measurement. The final waveform at equivalent waveform iteration 60 is the same as the waveform at equivalent waveform iteration 56. This was repeated to indicate the end of the waveform optimization and to indicate the PAE value that will be used in the system after the optimization is completed.

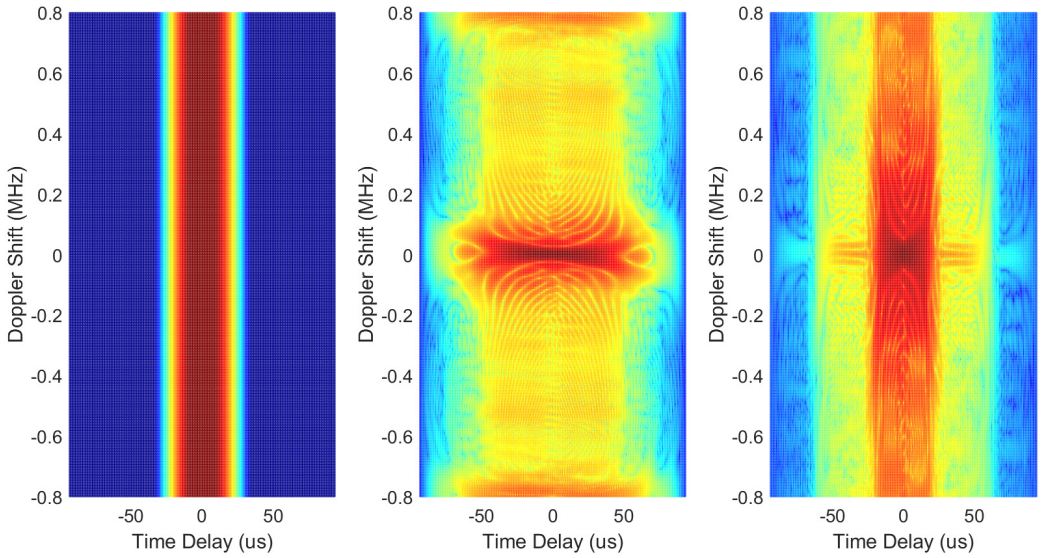

Figure 14. Ambiguity function comparison at equivalent waveform iteration 26. The minimization function is shown on the left, the sequential optimization waveform is shown in the middle, and the joint optimization waveform is shown on the right.

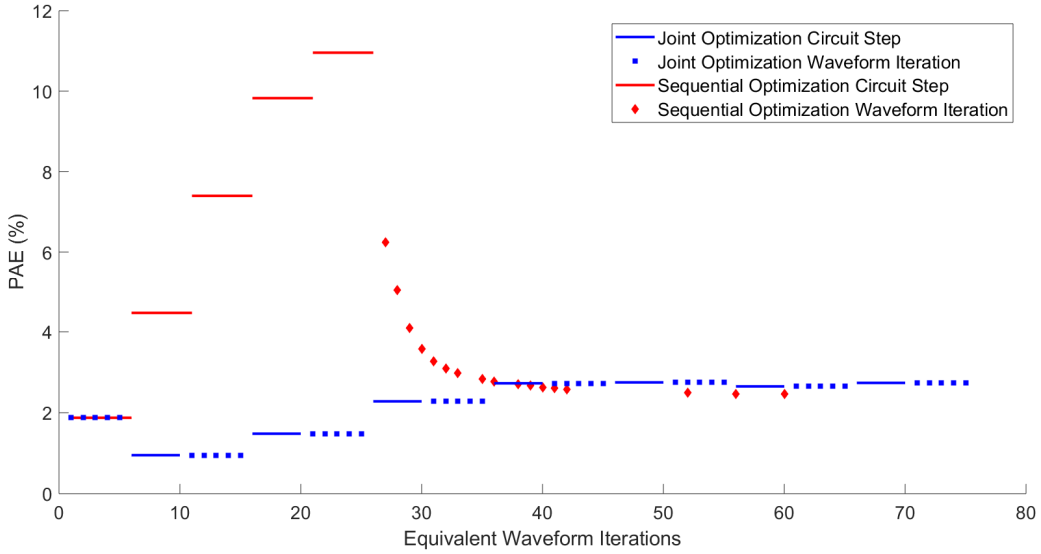

Figure 15. PAE Comparison with Equivalent Waveform Iterations. This shows how the PAE performs throughout the optimizations for a typical joint and sequential optimization trial.

Joint optimization again takes slightly longer than sequential optimization to complete the optimization. Since joint optimization begins with waveform optimization at the starting location, the first five measured waveform iterations are shown with the PAE at the starting location. This PAE is the same for joint and sequential optimizations because the waveforms that are first sent through the test setup are the same and are at the same values of Γ_L. Therefore, the PAE values are the same. After the first five measured waveform iterations, a circuit optimization is performed to find the next circuit step. Once the circuit step has been taken, five more waveform iterations are performed at this Γ_L point. For this reason, these waveform iterations are shown at the same vertical position as the circuit step that ended at that value of Γ_L.

As joint optimization continues to perform the optimization, the PAE continues until about equivalent waveform iteration 35, where the values start to peak. From this point, the waveform continues to be optimized, leading to waveforms that better meet all parameters. By the end of the search, joint optimization yields a higher PAE value that demonstrates a good tradeoff between circuit and waveform parameters, with the final Γ_L for joint optimization differing from the final Γ_L position for sequential optimization. After the circuit optimization converges, five more waveform iterations are performed to fine tune the waveform for the final Γ_L value, which causes a small increase in the PAE.

The S_m comparison for joint circuit and waveform optimization is shown in Figure 16. Sequential optimization, again, begins with circuit optimization. During the circuit optimization, the S_m values never get very close to 0 dB, since the starting waveform has a very narrow bandwidth, with a high PAE and low S_m. As the circuit search gets closer to the final value for Γ_L, the S_m increases. Once the waveform

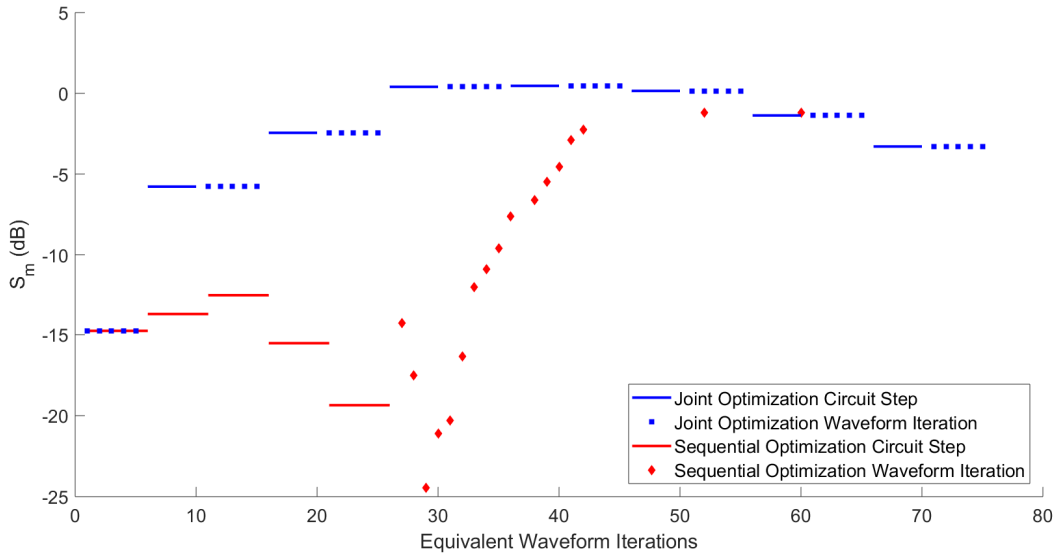

Figure 16. S_m Comparison with Equivalent Waveform Iterations. This shows how the Sm performs throughout the optimizations for a typical joint and sequential optimization trial.

optimization begins from the final Γ_L value, the S_m value gets closer to 0 dB, as the optimization gets closer to the range radar minimization template. The range radar minimization template forces the optimization to create a narrow pulse in the time domain, which leads to a wideband waveform that pushes the boundaries of the spectral mask. Again, the S_m value during the waveform optimization is measured whenever a waveform with a lower least squares distance is recorded. As shown in the graph, the optimization never goes above 0 dB, meaning that the optimization is always spectrally compliant.

Unlike sequential optimization, joint optimization starts with a set of waveform iterations. Again, these are placed at the same point as the starting S_m value for sequential optimization since they are both at the same Γ_L value and use the same waveform. Once joint optimization starts taking circuit steps, the S_m value starts to increase substantially, as the waveform optimization handles spectral compliance

throughout the optimization and since each circuit step is taken with a waveform that pushes the spectral mask. By equivalent waveform iteration 15, joint optimization is already really close to pushing the spectral mask, indicating that the waveform is starting to look like a range radar waveform. As the optimization continues, though, joint optimization goes just out of spectral compliance. Again, this is due to the limitations of the pre-distortion model. Because the model is not perfect, it is not able to account for all nonlinearities. However, how close the predistortion model is to the limit illustrates just how much the optimization pushes the spectral mask. Despite the issues with the pre-distortion model, the optimization was spectrally compliant after equivalent waveform iteration 56.

CHAPTER FIVE

Conclusions

When performing PAE optimization, traditional optimization schemes necessitate the use of a full load-pull, in which the PAE values are taken at multiple reflection coefficients around the Smith Chart. From there, the PAE maximum point is interpolated. However, load-pull optimization is extremely time consuming, as a full load-pull might need several hundred points to interpolate the PAE maximum accurately. The circuit optimization method discussed in the background of this thesis ensures that the PAE maximum can be found without the need for several hundred data points.

Waveform optimization is not typically applied to ambiguity function performance. However, the method of waveform optimization discussed earlier shows that it is possible. By creating minimization regions in the ambiguity function, the user can distinguish information such as velocity, relative size, and distance of a target to a high degree. Since the minimization function can be changed by the user, this optimization can be adapted to a wide variety of situations.

In this thesis, the circuit and waveform optimizations have been brought together for the reconfigurable radar transmitter application. Two different methods of combining the optimizations were explored: sequential optimization and joint optimization. For sequential optimization, the circuit optimization is completed to find the point on the Smith Chart with the highest PAE. After the circuit optimization is completed, a full waveform optimization is performed to match the signal to the ambiguity function minimization template and the other requirements. Joint optimization, on the other hand,

mixes the circuit and waveform optimization together. This optimization completes five waveform iterations for each step of the circuit optimization. This experiment shows the strong link that exists between the waveform and circuit optimizations. By taking advantage of the fact that the waveform impacts the PAE and the circuit impacts the ambiguity function, joint optimization allows for a higher PAE and better spectral compliance, all while the waveform is modified in ways that do not significantly affect the least squares distance. Additionally, joint optimization results in a waveform that has a better least squares distance from the ambiguity function template much earlier than sequential optimization. This means that joint optimization may allow the desired range/Doppler resolution much better than sequential optimization much earlier in the optimization process.

While joint optimization seems like the ideal optimization, it might not be the best for all scenarios. If the user has any *a priori* knowledge, sequential optimization might be more useful. Primarily, if the user knew the maximum PAE point, running sequential optimization could decrease the time needed to obtain a good circuit and waveform. In this case, the circuit optimization would run, but would only make minute adjustments. At this point, waveform optimization would take over. Joint optimization, on the other hand, would perform about the same as sequential optimization. Even though the circuit steps would be extremely small and the waveform would make small adjustments, a similar result would be achieved as in sequential optimization. However, joint optimization would take longer.

On the other hand, joint optimization would perform better if the user had no *a priori* knowledge and the information had to be extracted during the search. This would

yield the results that were discussed throughout this thesis, where joint optimization resulted in a higher PAE and spectral compliance. Joint optimization would also be extremely useful for dynamic environments, where any of the operating parameters (including operating temperature, frequency, power, and minimization function) change in real time, as joint optimization would not need to start over and would adequately take into consideration how the parameters changed.

Joint optimization of the circuit and waveform is useful for the next-generation radar, as this radar is based upon a dynamic environment, where environmental parameters can be modified in real time without requiring user input. By employing joint circuit and waveform optimization, the parameters can be modified without the need to start the optimization over with a full load-pull. This will be useful in the field, where joint circuit and waveform optimization can help save time and prevent targets from going undetected during the system's "down time".

Future Work

There is plenty of room for improving joint optimization. In the future, joint optimization will be applied to different load-pull tuners. The algorithm was designed so that it requires only a few lines of code changes to work with different tuners. For example, the Maury Microwave tuner used in this thesis is capable of reaching all parts of the Smith Chart. If a tuner is not capable of reaching the entire Smith Chart, the algorithm will need to restrict the search to within the characterized region. Additionally, another future step for joint optimization would be the implementation of a more advanced predistortion model, perhaps a neural network predistortion method. This will allow joint optimization to account for all the different nonlinearities of any amplifier.

This is necessary for field application, as it would ensure spectral compliance of the waveforms throughout the optimization. Lastly, a dynamic spectral mask can be implemented. This is necessary for the next-generation radar, as the spectral mask will need to change in real time.

BIBLIOGRAPHY

[1] AT&T Inc., "AT&T Files Public Interest Statement With FCC on T-Mobile Acquisition," 21 April 2011. [Online]. Available: https://www.att.com/gen/press-room?pid=19743&cdvn=news&newsarticleid=31838. [Accessed 14 March 2018].

[2] Federal Communications Commission, "National Broadband Plan," [Online]. Available: https://www.fcc.gov/general/national-broadband-plan. [Accessed 3 January 2018].

[3] M. Fellows, "Waveform and Circuit Optimizations to Provide Spectral Compliance for Cognitive Radar," 2014.

[4] M. Fellows, "Multidimensional Power Amplifier Circuit Optimizations for Adaptive Radar," 2017.

[5] M. Fellows, C. Baylis, J. Martin, L. Cohen and R. Marks, "Direct algorithm for the Pareto load-pull optimisation of power-added efficiency and adjacent-channel power ratio," *IET Radar, Sonar & Navigation,* vol. 8, no. 9, pp. 1280-1287, December 2014.

[6] M. Fellows, C. Baylis, L. Cohen and R. Marks, "Real-Time Load Impedance Optimization for Radar Spectral Mask Compliance and Power Efficiency," *IEEE Transactions on Aeorspace and Electronic Systems,* vol. 51, no. 1, pp. 591-599, January 2015.

[7] M. Fellows, M. Flachsbart, J. Barlow, J. Barkate, C. Baylis, L. Cohen and R. Marks, "Optimization of Power Amplifier Load Impedance and Chirp Wave-form Bandwidth for Real-Time Reconfigurable Radar," *IEEE Transactions on Aerospace and Electronic Systems,* vol. 51, no. 3, pp. 1961-1971, July 2015.

[8] J. Sevic, K. Burger and M. Steer, "A novel envelope-termination load-pull method for ACPR optimization of RF/microwave power amplifiers," in *IEEE MTT-S International Microwave Symposium Digest*, Baltimore, 1998.

[9] C. Baylis, L. Dunleavy, S. Lardizabal, R. Marks II and A. Rodriguez, "Efficient Optimization Using Experimental Queries: A Peak-Search Algorithm for Efficient Load-Pull Measurements," *Journal of Advanced Computational Intelligence and Intelligent Informatics,* vol. 15, no. 1, pp. 13-20, January 2011.

[10] H.-S. Chen, Y.-K. Hsieh and L.-H. Lu, "A 5.5-GHz multi-mode power amplifier with reconfigurable output matching network," in *2015 IEEE Radio Frequency Integrated Circuits Symposium (RFIC)*, Phoenix, 2015.

[11] D. Qiao, R. Molfino, S. Lardizabal, B. Pillans, P. Asbeck and G. Jerinic, "An intelligently controlled RF power amplifier with a reconfigurable MEMS-varactor tuner," *IEEE Transactions on Microwave Theory and Techniques,* vol. 53, no. 3, pp. 1089-1095, 2005.

[12] J.-S. Fu and A. Mortazawi, "Improving Power Amplifier Efficiency and Linearity Using a Dynamically Controlled Tunable Matching Network," *IEEE Transactions of Microwave Theory and Techniques,* vol. 56, no. 12, pp. 3239-3244, 2008.

[13] J.-R. Perez-Cisneros, J. de Mingo, P. Carro, P. Garcia-Ducar, C. Mateo, A. Valdovinos and C. Sanchez-Perez, "2-D Optimization Methodology for Reconfigurable Transmitters by Tunable Matching Networks," *IEEE Transactions on Circuits and Systems II: Express Briefs,* vol. 64, no. 11, pp. 1277-1281, 2017.

[14] A. Semnani, M. Abu Khater, Y. Wu and D. Peroulis, "An Electronically-Tunable High-Power Impedance Tuner with Integrated Closed-Loop Control," *IEEE Microwave and Wireless Components Letters,* vol. 27, no. 8, pp. 754-756, 2017.

[15] N. Kingsley and J. Guerci, "Adaptive Amplifier Module Technique to Support Cognitive RF Architectures," in *Proceedings of the 2014 IEEE Radar Conference*, Cincinnati, 2014.

[16] J. Martin, C. Baylis, L. Cohen, J. de Graaf and R. Marks II, "A Peak-Search Algorithm for Load-Pull Optimization of Power-Added Efficiency and Adjacent-Channel Power Ratio," *IEEE Transactions on Microwave Theory and Techniques,* vol. 62, no. 8, pp. 1772-1783, August 2014.

[17] Y. Collette and P. Siarry, Multiobjective Optimization: Principles and Case Studies, Berlin: Springer, 2004.

[18] J. Barkate, M. Flachsbart, Z. Hays, M. Fellows, J. Barlow, C. Baylis, L. Cohen and R. Marks, "Fast Simultaneous Optimization of Power Amplifier Input Power and Load Impedance for Power-Added Efficiency and Adjacent-Channel Power Ratio Using the Power Smith Tube," *IEEE Transactions on Aerospace and Electronic Systems,* vol. 52, no. 2, pp. 928-937, April 2016.

[19] P. Woodward, Probability and Information Theory with Applications to Radar, New York: Pergamon Press, 1953.

[20] D. Eustice, C. Baylis, L. Cohen and R. Marks II, "Waveform Synthesis via Alternating Projections with Ambiguity Function, Peak-to-Average Power Ratio, and Spectrum Requirements," in *2016 IEEE Radio and Wireless Symposium*, Austin, Texas, 2016.

[21] D. Eustice, C. Baylis, C. Latham, R. Marks II and L. Cohen, "Optimizing Radar Waveforms Using Generalized Alternating Projections," in *2015 Texas Symposium on Wireless and Microwave Circuits and Systems*, Waco, Texas, 2015.

[22] D. Eustice, C. Latham, C. Baylis, R. Marks II and L. Cohen, "Amplifier-in-the-Loop Adaptive Radar Waveform Synthesis," *IEEE Transactions on Aerospace and Electronic Systems,* vol. 53, no. 2, pp. 826-836, April 2017.

[23] R. J. Marks II, Handbook of Fourier Transforms & Its Applications, New York: Oxford University Press, 2009.

[24] A. Grebennikov, RF and microwave power amplifier design, New York: McGraw-Hill Professional, 2005.

[25] C. Chen and P. Vaidyanathan, "MIMO Radar Waveform Optimization With Prior Information of the Extended Target and Clutter," *IEEE Transactions on Signal Processing,* vol. 57, no. 9, pp. 3533-3544, September 2009.

[26] C. Wilcox, The synthesis problem for radar ambiguity functions, Institute for Mathematics and Its Applications, 1960.

[27] S. Sussman, "Least-square synthesis of radar ambiguity functions," *IRE Transactions on Information Theory,* vol. 8, no. 3, pp. 246-254, 1962.

[28] J. Wolf, G. Lee and C. Suyo, "Radar Waveform Synthesis by Mean Square Optimization Techniques," *IEEE Transactions on Aerospace and Electronic Systems,* Vols. AES-5, no. 4, pp. 611-619, 1969.

[29] I. Gladkova and D. Chebanov, "On a new extension of wilcox's method," *WSEAS Transactions on Mathematics,* vol. 3, no. 1, 2004.

[30] I. Gladkova and D. Chebanov, "On the synthesis problem for a waveform having a nearly ideal ambiguity surface," in *Proceedings of the International Conference RADAR 2004*, 2004.

[31] M. Kassab, M. Lesturgie and J. Fiorina, "Alternate projections technique for radar waveform design," in *Proceedings of International Radar Conference*, 2009.

[32] Y. Yang, R. Blum, Z. He and D. Fuhrmann, "MIMO Radar Waveform Design via Alternating Projection," *IEEE Transactions on Signal Processing,* vol. 58, no. 3, pp. 1440-1445, 2010.

[33] Y. Liu, H. Meng, G. Li and X. Wang, "Range-velocity estimation of multiple targets in randomised stepped-frequency radar," *Electronics Letters,* vol. 44, no. 17, pp. 1032-1034, 2008.

[34] S. Blunt, J. Jakabosky, M. Cook, J. Stiles, S. Seguin and E. Mokole, "Polyphase-coded FM (PCFM) radar waveforms Part II: Optimization," *IEEE Transactions on Aerospace and Electronic Systems,* vol. 50, no. 3, pp. 2230-2241, 2014.

[35] C. Latham, M. Fellows, C. Baylis, L. Cohen and R. Marks, "Radar waveform optimization for ambiguity function properties and dynamic spectral mask requirements based on communication receiver locations," in *Radio and Wireless Symposium*, Phoenix, 2017.

[36] Y. Nijsure, Y. Chen, P. Rapajic, C. Yuen, Y. Chew and T. Qin, "Information-theoretic algorithm for waveform optimization within ultra wideband cognitive radar network," in *2010 IEEE International Conference on Ultra-Wideband (ICUWB)*, Nanjing, China, 2010.

[37] J. Jakabosky, P. Anglin, M. Cook, S. Blunt and J. Stiles, "Nonlinear FM waveform design using marginal Fisher's information within the CPM framework," in *IEEE Radar Conference*, Kansas City, 2011.

[38] J. Jakabosky, S. Blunt, M. Cook, J. Stiles and S. Seguin, "Transmitter-in-the-loop optimization of physical radar emissions," in *IEEE Radar Conference*, Atlanta, 2012.

[39] S. Seguin, J. Jakabosky and S. Blunt, "Hardware-in-the-loop radar waveform optimization using radiated emissions," in *IEEE International Symposium on Electromagnetic Compatibility (EMC)*, Denver, 2013.

[40] S. Blunt, M. Cook, J. Jakabosky, J. de Graaf and E. Perrins, "Polyphase-coded FM (PCFM) radar waveforms, part I: implementation," *IEEE Transactions on Aerospace and Electronic Systems,* vol. 50, no. 3, pp. 2218-2229, 2014.